Iranian Polymer Journal (2019) 28:301–312
https://doi.org/10.1007/s13726-019-00700-y

ORIGINAL RESEARCH

Antifouling behaviour of PVDF/TiO_2 composite membrane: a quantitative and qualitative assessment

Zeenat Arif[1] · Naresh Kumar Sethy[1] · Lata Kumari[2] · Pradeep Kumar Mishra[1] · Bhawna Verma[1]

Received: 13 November 2018 / Accepted: 10 March 2019 / Published online: 14 March 2019

Abstract

The composite membranes of PVDF/TiO_2 were prepared by a phase-inversion technique. Different amounts of TiO_2 with respect to the weight of the polymer were incorporated in the casting solution to study qualitatively and quantitatively the antifouling property of the membrane. The membrane morphology was studied using a high-resolution scanning electron microscopy and atomic force microscopy, whereas the crystalline nature was studied using X-ray diffraction method. The interfacial interactions between foulants and TiO_2 immobilized membranes were also evaluated using the extended Derjaguin–Landau–Verwey–Overbeek (XDLVO) approach. The XDLVO theory revealed an increase in repulsive interactive energy barrier with an increase in TiO_2 loading, thus causing to improve the antifouling property of the membrane. Intercalation of TiO_2 nanoparticles efficiently improved the porosity and wettability of the polymeric membranes, which could be confirmed by the contact angle analyzer analysis. The modified PVDF membranes exhibited excellent antimicrobial properties against Gram-negative *Escherichia coli* as confirmed from the halo zone and activity test. The permeation experimental results also showed high protein rejection of bovine serum albumin and humic acid (foulant) for membranes with optimum TiO_2 loading of 0.01 g/g of PVDF polymer. However, at a concentration of 0.02 g TiO_2/g of PVDF a negative effect on the membrane property was observed due to the former non-uniform distribution.

Keywords Hydrophilicity · Fouling · Permeability · Membrane · Antibacterial

Introduction

Membrane separation technology is widely used for getting potable and industrial grade water for various applications [1, 2]. Fouling of membrane affects the hydraulic permeability and forces frequent replacement of the fouled membrane thereby increasing the overall cost of the process [3, 4]. Therefore, the membrane fouling has been a subject of interest for researchers since long [5]. The biofouling of the membrane is initiated by the adhesion, growth, and multiplication of one or more bacterial species and/or flocs onto the membrane surface, which eventually leads to the formation of a cake layer on the membrane surface [6]. In recent studies, it has been concluded that the prime factor affecting the membrane fouling is its interfacial property [7] which controls membrane-foulant interactions hence, the adsorption of foulant on the membrane surface [7, 8]. Hydrophilicity and hydrophobicity are the prime factors behind fouling, and it has been recognized that hydrophilic membranes are less prone to fouling compared to hydrophobic membranes [9, 10]. Based on this information, strategies such as graft polymerization, chemical grafting, and surface coating have been considered to improve the surface hydrophilicity and modify membrane characteristics [2]. The main disadvantages of these approaches include weak interaction between the polymer and additives (blending) which affects the long-term durability or instability of the coated layer (surface modification) causing its release from the membrane [2].

Among various methods used, incorporation of inorganic particles into the polymer matrix to form a composite membrane is an effective approach to enhance membrane hydrophilicity and antifouling property [11]. Different inorganic nanomaterials, such as TiO_2 [12, 13], SiO_2 [14], Al_2O_3 [15], graphene oxides [16], and carbon nanotubes [17] have been widely used to fabricate composite membranes. However,

✉ Zeenat Arif
zeenata.rs.che15@itbhu.ac.in

[1] Department of Chemical Engineering and Technology, Indian Institute of Technology (BHU), Varanasi, India

[2] Department of Chemistry, Indian Institute of Technology (BHU), Varanasi, India

nano-sized TiO_2, due to its superior hydrophilicity, antibacterial property, and chemical stability has received much attention [18]. Addition of TiO_2 nanoparticles improves the system's antifouling property due to changes in hydrophilicity, porosity, zeta potential, and surface roughness [3].

Further, preparation of anti-biofouling membranes by coupling antimicrobial materials with polymeric matrix has also attracted the attention of many researchers in both academia and industry. There are two interesting approaches to kill bacteria before colonization: (1) release killing, and (2) contact killing [19]. Leaching of antibacterial agents on the membrane surface is termed as "release killing", but there is continuous depletion of biomaterial that may cause environmental risks and significantly reduces the antibacterial efficiency. As a result, the need for developing composite membranes with the contact-killing surface and stable and long-term anti-biofouling activities has attracted the attention of researchers [19]. Inorganic metal oxides are being more preferred over organic antimicrobial agents due to their stability, robustness, and long shelf life [20]. Titanium dioxide (TiO_2) has been the widely used nanomaterial because of its stability, hydrophilicity, nontoxic, and antifouling properties [21–23].

Most of the available published works have reported the experimental methods to characterize the antifouling property of the membrane. A systematic investigation of the interaction of nanoparticles in improving the antifouling property is rarely known. In this work, the efficacy of these membranes has also been investigated by using extended Derjaguin–Landau–Verwey–Overbeek (XDLVO) theory, for the first time. The experimental results are compared with the theoretical predictions approach for evaluating the antifouling property of the membranes and its quality changes by the addition of nanoparticles.

Further the effect of loading of TiO_2 nanoparticles on the antifouling property of PVDF membrane, obtained by phase-inversion membranes, is evaluated by measuring the pure water flux and rejection efficiency of bovine serum albumin (BSA) and humic acid (HA). The bactericidal behaviour and antimicrobial effects are studied using Gram-negative bacteria (*Escherichia coli*).

XDLVO theory

The extended Derjaguin–Landau–Verwey–Overbeek (XDLVO) theory explains the exact role of hydrophilicity/hydrophobicity and all other physiochemical factors on the membrane surface energy (interfacial interaction between membranes and foulants) [3, 24]. The theory describes that the attachment of foulant with membrane surface is due to three types of interactions: (1) Lifshitz–van der Waals (LW), (2) polar or Lewis acid–base (AB), and (3) electrostatic energy (EL) [25–27] interactions.

The XDLVO theory considers the attachment of foulant to the membrane surface by evaluating the interaction of surface energies [28]. According to Oss [29], the total free energy of adhesion is the result of contribution of these three parameters and is expressed as:

$$U_{\mathrm{mbc}}^{\mathrm{XDLVO}} = U_{\mathrm{mbc}}^{\mathrm{LW}} + U_{\mathrm{mbc}}^{\mathrm{EL}} + U_{\mathrm{mbc}}^{\mathrm{AB}}, \tag{1}$$

where $U_{\mathrm{mlc}}^{\mathrm{XDLVO}}$ is the total interfacial free energy between the membrane and foulant, $U_{\mathrm{mbc}}^{\mathrm{LW}}$, $U_{\mathrm{mbc}}^{\mathrm{EL}}$, and $U_{\mathrm{mbc}}^{\mathrm{AB}}$ represent individual components of the total interfacial energy, whereas m, b and c represent membrane, bulk liquid (water) and foulant (BSA), respectively. The individual energy is calculated using Eqs. (2), (3), and (4) as follows:

$$U_{\mathrm{mbc}}^{\mathrm{LW}} = 2\pi\Delta G_{h_{\mathrm{o}}}^{\mathrm{LW}} h_{\mathrm{o}}^2 \frac{a}{h}, \tag{2}$$

$$U_{\mathrm{mbc}}^{\mathrm{AB}} = 2\,\pi a\,\lambda\Delta G_{h_{\mathrm{o}}}^{\mathrm{AB}} \exp\frac{(h_{\mathrm{o}} - h)}{h}, \tag{3}$$

$$U_{\mathrm{mbc}}^{\mathrm{EL}} = \pi\varepsilon a\left\{2\zeta_{\mathrm{c}}\zeta_{\mathrm{m}}\ln\left(\frac{1+\mathrm{e}^{-kh}}{1-\mathrm{e}^{-kh}}\right) + (\zeta_{\mathrm{c}}{}^2 + \zeta_{\mathrm{m}}{}^2)\ln\left(1-\mathrm{e}^{-2kh}\right)\right\}, \tag{4}$$

where a is radius of foulant (BSA), h is the separation distance between membrane and foulant, h_{o} is minimum separation distance (0.158 nm), λ is decay length (value taken as 0.6 nm for aqueous solution) [30], ζ_{c}, ζ_{m} are the zeta potential of foulant and membrane, respectively, k is the inverse Debye screening length, whereas $\Delta G_{h_{\mathrm{o}}}^{\mathrm{LW}}$ and $\Delta G_{h_{\mathrm{o}}}^{\mathrm{AB}}$ can be calculated using Eqs. (5) and (6), respectively, as follows:

$$\Delta G_{h_{\mathrm{o}}}^{\mathrm{LW}} = 2\left(\sqrt[2]{\gamma_{\mathrm{b}}^{\mathrm{LW}}} - \sqrt[2]{\gamma_{\mathrm{m}}^{\mathrm{LW}}}\right)\left(\sqrt[2]{\gamma_{\mathrm{f}}^{\mathrm{LW}}} - \sqrt[2]{\gamma_{\mathrm{b}}^{\mathrm{LW}}}\right), \tag{5}$$

$$\begin{aligned}\Delta G_{h_{\mathrm{o}}}^{\mathrm{AB}} = {} & 2\sqrt[2]{\gamma_{\mathrm{b}}^{+}}\left(\sqrt[2]{\gamma_{\mathrm{m}}^{-}} - \sqrt[2]{\gamma_{\mathrm{c}}^{-}} - \sqrt[2]{\gamma_{\mathrm{b}}^{-}}\right) \\ & + 2\sqrt[2]{\gamma_{\mathrm{b}}^{-}}\left(\sqrt[2]{\gamma_{\mathrm{m}}^{+}} - \sqrt[2]{\gamma_{\mathrm{c}}^{+}} - \sqrt[2]{\gamma_{\mathrm{b}}^{+}}\right) \\ & - 2\left(\sqrt[2]{\gamma_{\mathrm{m}}^{+}\gamma_{\mathrm{c}}^{-}} + \sqrt[2]{\gamma_{\mathrm{m}}^{-}\gamma_{\mathrm{c}}^{+}}\right),\end{aligned} \tag{6}$$

where γ^{LW}, γ^{+}, γ^{-} are LW component, electron acceptor and donor parameter, in the order given. The surface tension of membrane ($\gamma_{\mathrm{m}}^{\mathrm{LW}}, \gamma_{\mathrm{m}}^{-}, \gamma_{\mathrm{m}}^{+}$) and BSA were quantified using extended Young's equation. This equation shows the relationship between contact angle of a liquid and surface tension parameter of both liquid and solid surfaces and is evaluated using Eq. (7):

$$(1+\cos\theta)\gamma_{\mathrm{l}}^{\mathrm{TOT}} = 2\left(\sqrt[2]{\gamma_{\mathrm{s}}^{\mathrm{LW}}\gamma_{\mathrm{l}}^{\mathrm{LW}}} + \sqrt[2]{\gamma_{\mathrm{s}}^{+}\gamma_{\mathrm{l}}^{-}} + \sqrt[2]{\gamma_{\mathrm{s}}^{-}\gamma_{\mathrm{l}}^{+}}\right), \tag{7}$$

where θ is the contact angle and γ_l^{TOT} is the sum of LW and AB and is calculated using Eq. (8):

$$\gamma_l^{TOT} = \gamma^{LW} + \gamma^{AB}. \quad (8)$$

The polar component γ^{AB} of the material is expressed by Eq. (9):

$$\gamma^{AB} = 2(\gamma^+\gamma^-)^{0.5}. \quad (9)$$

Experimental

Materials

Polyvinylidene fluoride (PVDF), *n*-methyl-2-pyrrolidone (NMP), and TiO_2 nanoparticles (Degussa P25 (25 nm), a hydrophilic metal oxide) were purchased from Sigma-Aldrich. Diiodomethane, glycerol, nutrient broth (NB) as media and nutrient agar (NA) used were obtained from High Media (Bombay), bovine serum albumin (BSA) and Humic acid (HA) were obtained from SDFCL (Bombay), and phosphate buffer saline (PBS) was obtained from Merck. Double distilled water (DD) used in all experiments was prepared in the laboratory.

Synthesis of PVDF/TiO_2 composite membranes

The PVDF composite membranes were synthesized by a phase-inversion method. The PVDF pellets were dried in an oven at 90 °C for 24 h. 4 g of the dried PVDF pellets was dissolved in 20 mL of organic solvent NMP using a magnetic stirrer and a temperature of around 65–70 °C to achieve a homogeneous solution. Simultaneously different quantities of TiO_2 were dispersed in 4 mL of NMP by sonication for 1 h. Each of these TiO_2 suspensions was mixed separately with 20 mL of PVDF, and these were then thoroughly mixed together with continuous stirring for 8 h at 65–70 °C to achieve a uniform suspension. This solution was subsequently cast as a film on a glass plate with a clearance of 200 µm and exposed to air for 30 s for partial evaporation of the solvent. The plates coated with the polymer-TiO_2 suspension were then placed in a water bath at ambient temperature (27 ± 1 °C) for 24 h for precipitation. The membranes were peeled off from the glass plates, washed and stored under water for further study. Membranes with different loading of TiO_2 are named as M1 (0 g TiO_2/g PVDF), M2 (0.005 gTiO_2/g PVDF), M3 (0.01 TiO_2/g PVDF) and M4 (0.02 TiO_2/g PVDF).

Physiochemical properties of membranes

Contact angle measurement

The wetting characteristic of the membranes was evaluated by measuring the contact angle of the composite membrane surface with a contact angle goniometer [KRUSS, Germany] using the sessile drop method. 3 µL droplet of distilled water was used as the probe liquid at the ambient temperature.

Morphological characterization

The Smart Lab X-Ray Diffractometer (Rigaku Smart Lab Powder type, without χ-cradle) was used for X-ray diffraction studies. The equipment operated at 18 kW and used a Rotating Anode XRD (1200–1800 K temperature) containing CuK_α radiation ($\lambda = 1.5406$ Å). The membrane surface was examined using a high-resolution scanning electron microscope (HRSEM, SUPRA 40, Zeiss). The membrane films were initially coated by sputtering with gold, and the photomicrographs were taken under very high vacuum. The scanning probe microscope (NTEGRA Prima) was used to detect the surface roughness of the synthesized membranes under the non-contact mode.

Antibacterial characteristics

Halo zone test

The antibacterial efficacy of PVDF/TiO_2 membranes was evaluated experimentally using the halo zone method. Prior to the tests, all the materials used were autoclaved at 120 °C for 1 h to ensure sterility. Cultivation of *E. coli* was carried out for 24 h in a conical flask containing the sterilized solution of NB (1.3 g NB/100 mL water) placed in an incubator maintained at 37 °C. During this period, the bacteria were fully grown, and then 100 µL of the bacterial suspension was spread over the NB agar plate composed of 1.3 g of NB and 2.3 g of NA in 100 mL distilled water. The UV-treated membrane pieces of approximately 1 cm diameter were now placed on the agar plates and again incubated at 37 °C for 24 h. The extent of inhibition zone formation around the membrane pieces indicated the antibacterial behaviour of the membranes [31, 32].

Bacterial growth

All glass-wares, the nutrient broth solution, and all other solutions were autoclaved at 120 °C for 60 min. The membrane pieces of known area (1 cm × 1 cm) were first rinsed three times with 0.01 M fresh sterile phosphate buffered saline (PBS, pH 7.4) followed by sterilization through UV irradiation for half an hour. A bacterial suspension (10^{-3}

cells/100 mL) was prepared in the sterile nutrient broth. The UV-treated membrane pieces were then immersed in the above suspension. Subsequently, the flasks containing pieces of different composite membranes and bacterial suspensions were incubated in a rotary shaker at 100–105 rpm at 37 °C in the absence of any light. The growth of *E. coli* was measured in terms of optical density at 600 nm (OD_{600}) [33] at several incubation times ($t = 0$, 6, 12, 18, and 24 h) using a spectrophotometer (SYSTRONICS, PC Based Double Beam Spectrometer 2202). Each reported value was obtained by averaging ten individual measurements. Data of the exponential growth phases were fitted using the pseudo-first-order kinetics:

$$\ln\left(x_t/x_0\right) = \mu t, \tag{10}$$

$$\tau_d = \ln 2/\mu, \tag{11}$$

where x_0 and x_t represent values of OD_{600} for the bacterial suspensions at 0 and t h, respectively, μ is the specific growth rate (h^{-1}), and τ_d represents the doubling time (h).

The adhesion and growth of *E. coli* on membrane surface were observed using a HRSEM (high-resolution scanning electron microscope).

Water permeation studies

The pure and composite PVDF membranes with the filtration area of 15.5 cm^2 were used in a flow filtration cell to test the fouling behaviour using BSA as the model foulant (1 g/L, pH 7.5). Initially, the synthesized membranes were compacted at 0.2 MPa to achieve a stable flux, and then a pure water flux Q_w (kg/m^2 h) was measured at 0.1 MPa for 1.5 h and then it was replaced by the BSA solution. Permeation of BSA was recorded as Q_F and concentrations of feed and permeates were evaluated using UV spectrophotometer by measuring the absorbance at 280 nm [34].

$$Q_w = M/(A \times t), \tag{12}$$

where M is the permeate mass (kg), A is the membrane area (m^2), and t is the permeation time (h). The rejection percentage of BSA was calculated from Eq. (13):

$$R = \left(1 - B_p/B_f\right) \times 100, \tag{13}$$

where B_p and B_f (mg/mL) are the concentrations of BSA in permeate and feed, respectively.

The fouled membranes were rinsed with water, and the water permeability was again measured as Q_{WR}. The regeneration test was carried out to analyze the recovery and self-cleaning ability of membranes which was calculated using Eq. (14):

$$FRR = Q_{WR}/Q_w \times 100, \tag{14}$$

where Q_{WR} is the water flux after each cycle (kg/m^2 h) and Q_w is the initial pure water flux (kg/m^2 h).

The filtration experiment with 5 mg/L HA at 0.2 MPa for 1.5 h was conducted to further evaluate the antifouling property of composite membrane, following the same procedure as described above by replacing BSA with HA. The water flux before and after contact with HA solution was measured, and flux decline was calculated in terms of relative fluxes.

Results and discussion

Physiochemical properties of the membrane

XRD analysis

The morphology of the membranes was studied using X-ray diffraction pattern as shown in Fig. 1. The PVDF has four different crystalline structures α, β, γ, and δ, where α-phase is the kinetically stable phase, and β-phase is the thermodynamically favoured phase [18]. At the diffraction angles 18.5° and 26.5°, the peak corresponds to α-phase, whereas at 20.5° for β-phase [19]. The additional two peaks for membranes M2, M3, and M4 with increasing intensity at 2 **Ø** equal 25.2° and 48.0° confirm the presence of anatase phase of TiO_2 with (101) and (200) planes [20] which provides a better antifouling behaviour. The major peak intensity of PVDF (20.5°) in PVDF/TiO_2 membranes is lower compared to those for pure PVDF membrane. This decrease in intensity is due to the intercalation of TiO_2 nanoparticles. The introduction of nanoparticles results in an amorphous region.

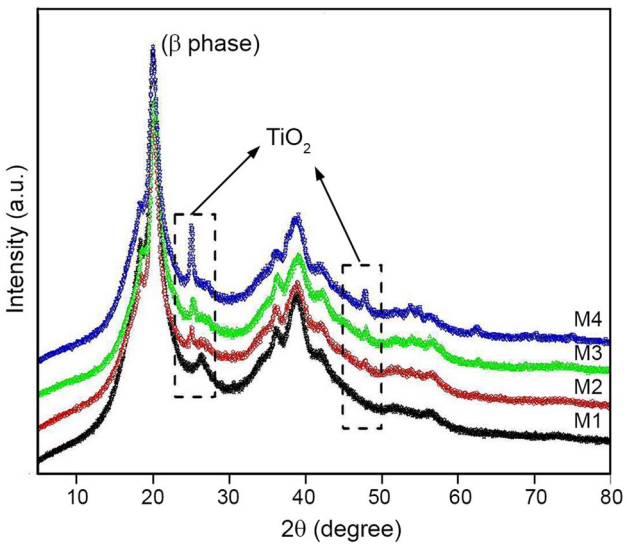

Fig. 1 XRD patterns of PVDF/TiO_2 membranes

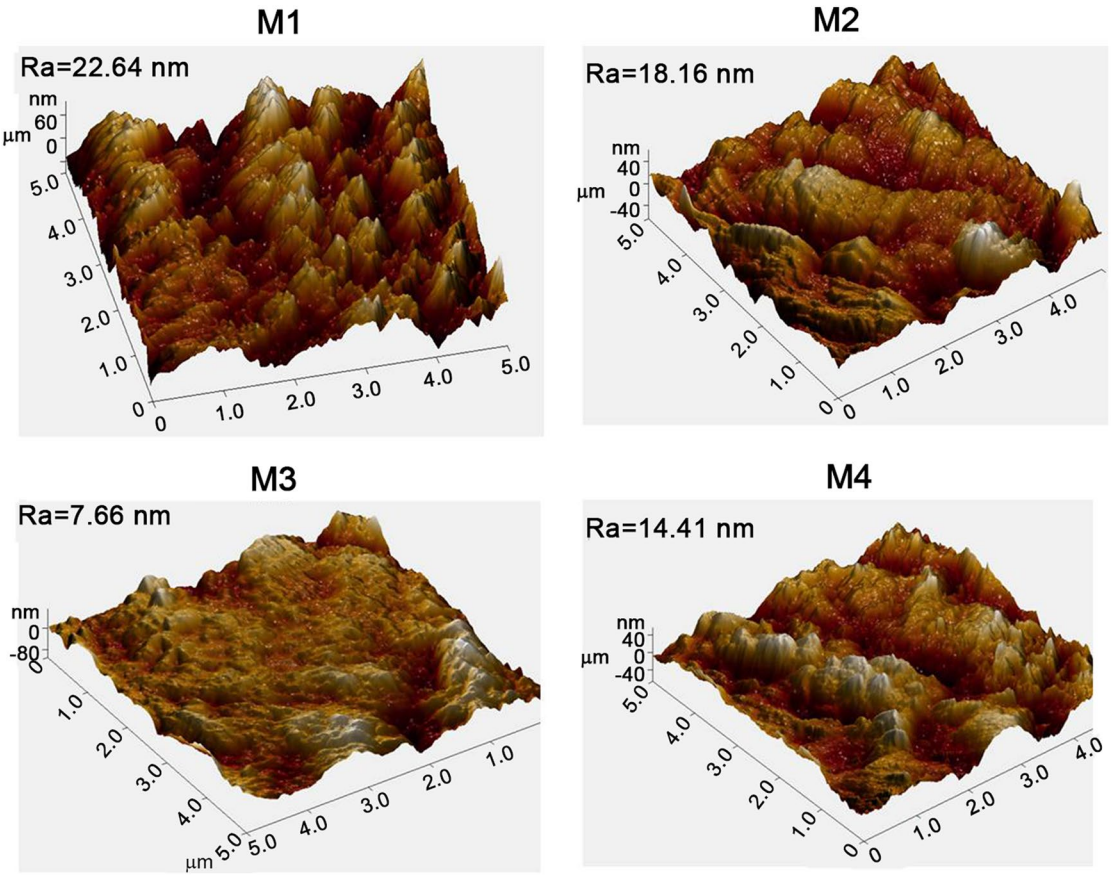

Fig. 2 3D AFM image of different PVDF composite membranes

AFM analysis

The AFM photomicrographs given in Fig. 2 show the effect of TiO_2 loading on the membrane surface roughness. In a 3D AFM image, the bright portion represents the highest peak on the membrane surface, whereas the dark portion represents valleys. It is a known fact that smoother the membrane surfaces the lesser will be the fouling tendency [35]. In case of membranes with a rough surface, accumulation of foulants will occur within the "valleys" and such membranes will foul easily. Figure 2 depicts that membrane M1 (no TiO_2) exhibits several large peaks and valleys, i.e., it has a very rough surface. The decrease in roughness parameter indirectly enhances the antifouling property of the polymeric membrane. Roughness is defined by three parameters: (1) mean roughness (Ra) defined as average deviation of the z values, which is half the average peak to valley depth, (2) root mean square roughness (Rq) which represents standard deviation of an entire z values, and (3) average of height (Rz) expressed as the difference of the largest positive and negative z values [3].

The values of these roughness parameters for different composite membranes are listed in Table 1, (AFM scanning area of 5 μm × 5 μm). The results indicate that surface roughness decreases with increase in the concentration of TiO_2, but the membrane M4 with the highest loading exhibits higher roughness; this is likely to be due to the presence of aggregated particles [36]. Excessive addition of TiO_2 particles in the matrix results in bumps formation hence, increases the peak value. Similar results are also reported in the literature [37, 38].

Table 1 Roughness parameter of PVDF and its composite membrane

Sample	Ra (nm)	Rq (nm)	Rz (nm)
M1	22.64	22.76	74.45
M2	18.16	23.68	61.94
M3	07.66	09.78	29.88
M4	14.41	17.03	43.88

Surface hydrophilicity and wetting ability of pure and composite membranes

The wetting ability of the polymeric membrane surface was determined by measuring the static contact angles.

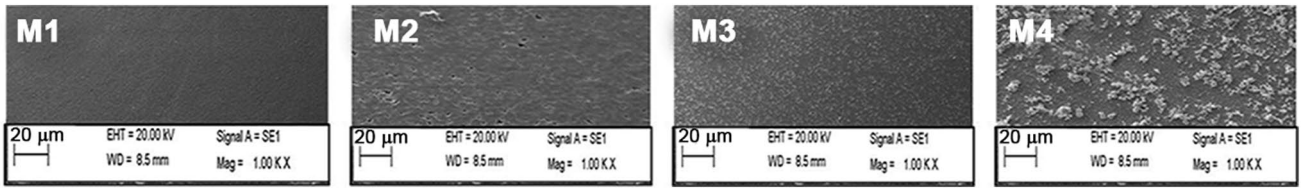

Fig. 3 SEM images of PVDF/TiO_2 composite membrane

Table 2 Contact angle value of three different probe liquids

Contact angle	Ultrapure water	Diiodomethane	Glycerol
M1	86.7	62.8	70.1
M2	78.2	57.9	63.8
M3	72.6	53.6	59.2
M4	74.8	55.1	61.7

Table 3 Surface tension values (mJ/m^2) of three probe liquids

Probe liquid	γ^{LW}	γ^+	γ^-	γ^{AB}	γ^{TOT}
Ultrapure water	22.1	25.5	25.5	50.7	72.8
Diiodomethane	50.8	0	0	0	50.8
Glycerol	34	3.92	57.4	30	64

The observed decrease in the value of contact angle for PVDF/TiO_2 membranes compared to pure PVDF membrane can be attributed to the high affinity of TiO_2 for water [39]. The contact angle of pure PVDF membrane (86.7°) is higher than that of PVDF/TiO_2 composite membranes and with an increase in TiO_2 loading from 0 to 0.01 g TiO_2/g PVDF it decreases from 86.7° (M1) to 72.6° (M3). These results are consistent with earlier reports [39, 40]. The wetting ability of membranes is a function of the surface hydrophilicity and roughness [41]. It was also observed that at high concentration of TiO_2 (M4 membrane), this value increases further; this may be attributed to the particle aggregation resulting in non-uniform distribution of particles within the membrane matrix [41] as shown in Fig. 3. This value indirectly gives an idea that hydrophilicity of composite membranes is enhanced due to the presence of hydrophilic TiO_2 particles hence, leads to an improvement in the antifouling property. Based on these data, the free energy and surface tension parameters were evaluated using equations defined in the XDLVO theory section.

XDLVO theory-based analysis of fouling behaviour

A better understanding of the fouling mechanism of the membranes can be obtained by estimating the physico-chemical interactions between the foulant and composite membrane. The surface tension parameters of membranes were calculated using the Young–Dupré equation using the measured contact angles of three different probe liquids with known parameters (Tables 2, 3, 4). The results show that the electron donor component (γ^-) value is always greater than the electron acceptor component (γ^+) value, indicating that all the membranes exhibit high electron donor mono-polarity that varies from 1.522 to 2.804 mJ/m^2. The results are consistent with the reported values [42]. It was also found that membrane M4 has the highest values of (γ^+) and (γ^{AB}) compared to other membranes, indicating high polar properties.

The high values of electron donor components (γ^-) for TiO_2-modified PVDF membranes indicate mono-polar hydrophilic surface due to the presence of hydrophilic TiO_2 nanoparticles.

The increase in γ^{TOT} with increasing TiO_2 loading in membranes means strong interfacial molecular affinity between the membrane and water molecules. A tightly bound formation of the steric-entropic barrier will restrain the interaction between the membrane surface and foulant, hence delays the fouling [43].

The individual surface free energy AB and LW parameters were calculated using Eqs. (5) and (6). The sum of these two energy components for any given material gives the free energy of cohesion (ΔG^{TOT}). It provides a quantitative perception regarding the hydrophilicity and hydrophobicity.

Table 4 Surface tension and surface free energy of membranes

Sample	γ^{LW}	γ^+	γ^-	γ^{AB}	γ^{TOT}	$\Delta G^{LW}_{h_o}$	$\Delta G^{AB}_{h_o}$	ΔG^{TOT}
M1	5.199	1.268	1.522	3.859	9.058	− 10.548	− 50.718	− 61.267
M2	5.464	1.280	2.328	5.959	11.423	− 10.298	− 42.906	− 53.204
M3	5.685	1.280	2.804	7.178	12.863	− 10.094	− 38.328	− 48.422
M4	5.609	1.649	2.231	7.358	12.967	− 10.163	− 41.963	− 52.126

The thermodynamic theory suggests that adhesion or attraction between two materials occurs when ΔG^{TOT} is negative. Higher the negative value stronger is the hydrophobicity; intensity in the attraction between membrane and foulant, hence more severe will be the membrane fouling.

It is also observed that ΔG^{TOT} is more negative for pure PVDF membrane, indicating it to be more hydrophobic and, hence, a stronger attraction between membrane and foulant [43]. The value increases on increasing the TiO_2 loading, and is significant for membrane M3, indicating a less force of attraction between foulant (BSA) and the membrane. Further increase in TiO_2 loading increases the agglomeration of the particle, resulting in a reduction in free energy of cohesion for PVDF/TiO_2 membranes. These values were further used to calculate the individual interaction energy parameters, based on which total interaction energy U_{mlc}^{XDLVO} was evaluated. The plots of interaction energy as a function of separation distance are shown in Fig. 4. The figure explains the effect of interaction energy on membrane fouling. It is seen that as the separation distance increases the interaction energy gradually approaches zero. The figure also predicts that the foulant needs to overcome the repulsive force to attach to the membrane surface. The higher the repulsive barrier, the harder will be for the foulant to achieve attachment [3]. For the membranes used in this work the energy barrier followed the order M3 > M4 > M2 > M1. As a result, deposition or blocking of membrane surface for M3 is minimal. Thus it is seen that improving the membrane hydrophilicity by adding TiO_2 will diminish the membrane fouling [19].

These results provide a quantitative picture of the interfacial interactions between foulants and membrane based on XDLVO theory. From the contact angle values and the results of XDLVO theory, it can be said that fouling of membrane can be mitigated by strengthening the interface polarity and hydrophilicity.

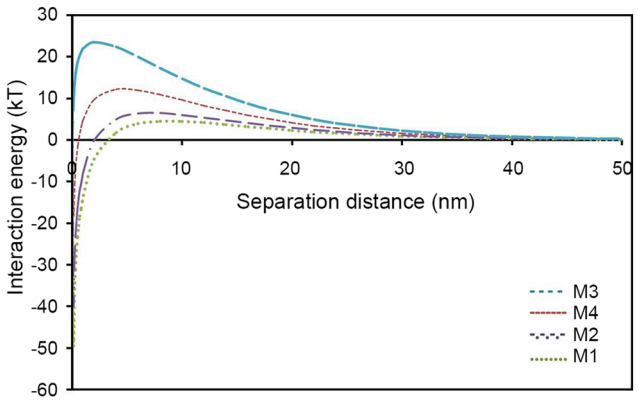

Fig. 4 Variation of interaction energy between membrane and BSA

Antibacterial property

Halo zone test

The halo zone tests were used to qualitatively investigate the antibacterial property of pure PVDF and TiO_2-incorporated membranes against Gram-negative bacteria (*E. coli*) after 24 h of incubation at 37 °C. Figure 5 shows the strength of the inhibition zone, an area around membrane piece without any growth of bacteria after 24 h. These figures depict that pristine PVDF (M1) being hydrophobic does not exhibit inhibition zone hence has no antibacterial activity. All membranes with TiO_2 exhibit inhibition zone formation, but the zones for M3 and M4 membranes are more prominent. Thus, it can be said that the inherent antibacterial property of TiO_2 protects the membrane from fouling by not allowing bacteria to grow in the nearby region.

Bacterial growth

The Gram-negative (*E. coli*) bacteria were used to test the antimicrobial activity of pristine PVDF and PVDF/TiO_2 membranes. The OD_{600} values during and after 24 h incubation are shown in Fig. 6. These figures indicate that membranes M3 and M4 exhibit significant inhibition capacity towards *E. coli* strains.

The viability of bacteria on the pure and composite membrane surface before and after incubation for 24 h was determined by HRSEM. Figure 7 depicts the adhesion and

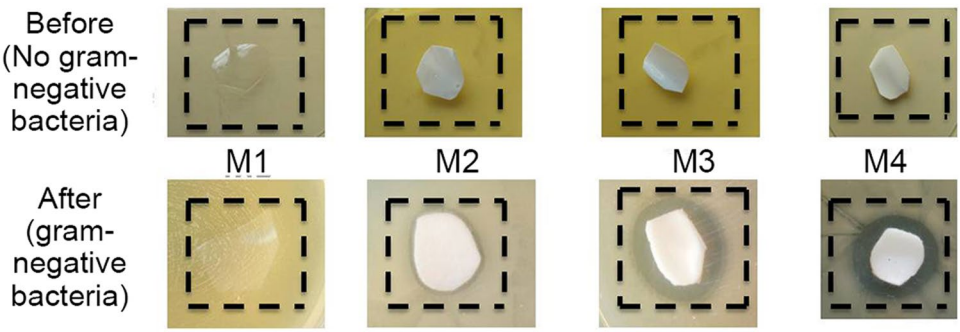

Fig. 5 Inhibition zone formation for different PVDF composites membranes

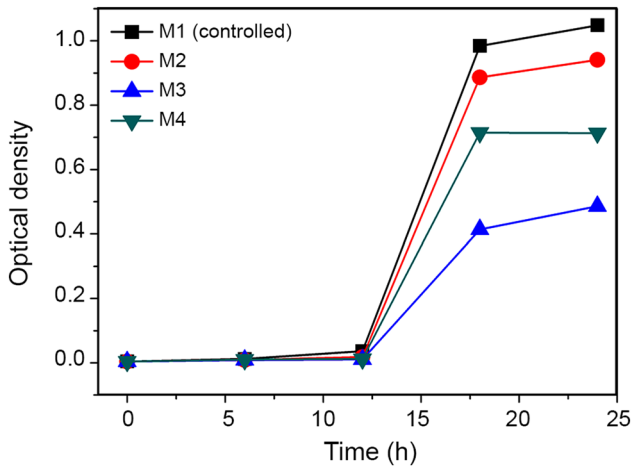

Fig. 6 OD_{600} value of the M1 (control, no TiO_2), M2, M3 and M4 incubated for 24 h

growth of *E. coli* on pure PVDF and composite membranes. It is clear that the surface of membrane M1 is covered with a large number of bacteria while that of membrane M3 with the least number. This can be attributed to the disruption of the cell wall due to the presence of nanoparticles [44]. These results are consistent with the results of AFM and contact angle values since membrane M1 having a high value of roughness and being hydrophobic is more susceptible to fouling compared to the membrane M3 with the lowest roughness value as shown in the AFM result in Fig. 2 and the hydrophilic characteristics. The HRSEM images exhibit the growth behaviour of bacteria and it is observed that the trend for the growth of bacteria over the membrane surface is similar to that observed for the biocidal activities obtained from OD_{600} measurements.

The cell proliferation of *E. coli* was studied for the exponential growth phase for 3–24 h to see the inhibition by nanocomposite membrane. The results reveal that specific growth rate (μ) of *E. coli* is very high in the presence of pristine PVDF and decreases dramatically with an increase in TiO_2 loading. The increase in the doubling time τ_d (Fig. 8) was also observed. The optimal growth inhibition is not observed for the highest TiO_2 loading (M4 membrane), due to agglomeration of particle which leads to the availability of less active sites for killing *E. coli* cells.

At low concentrations, TiO_2 does not cover the entire membrane surface as a result, some bacteria grow. The membrane M3 results in intimate contact between TiO_2 particles and the bacteria which affects the bacterial cell wall readily and leads to enhancement in the antibacterial effect [45]. Antibacterial activity is reduced for membrane M4. At higher concentrations, due to particle agglomeration, the surface is not completely covered with TiO_2 nanoparticles leaving some space for the bacteria to grow [46]. Our study has confirmed that TiO_2 exhibits anti-bactericidal activity, and the result is consistent with that of Rahimpour et al. [45] as well as aggregation of TiO_2 NPs results in the loss of available surface area for reducing fouling.

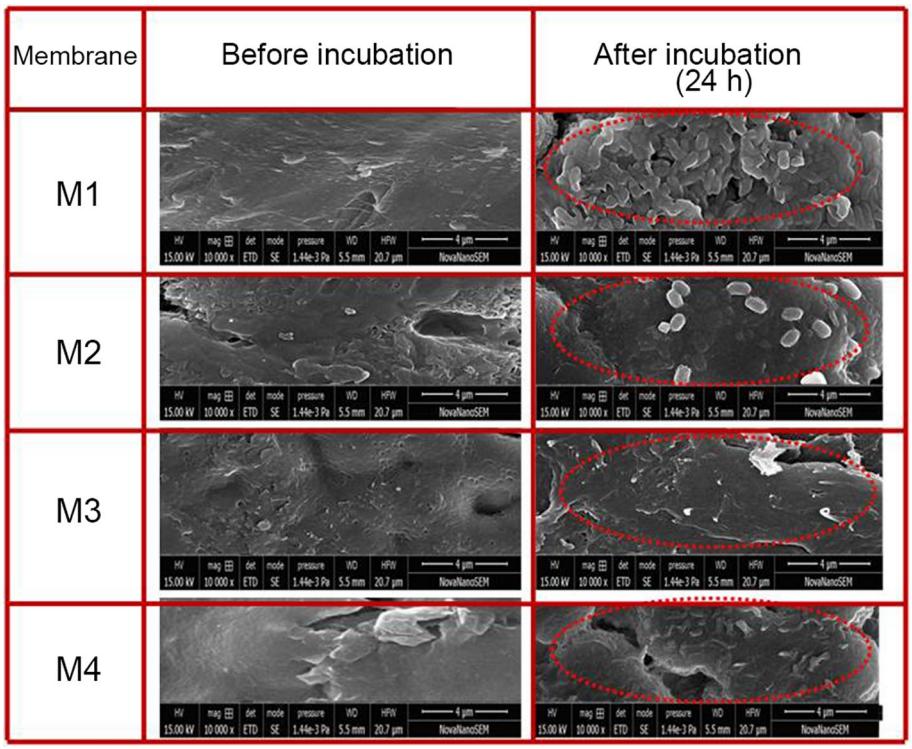

Fig. 7 HRSEM images of PVDF–TiO_2 membranes before and after bacterial growth

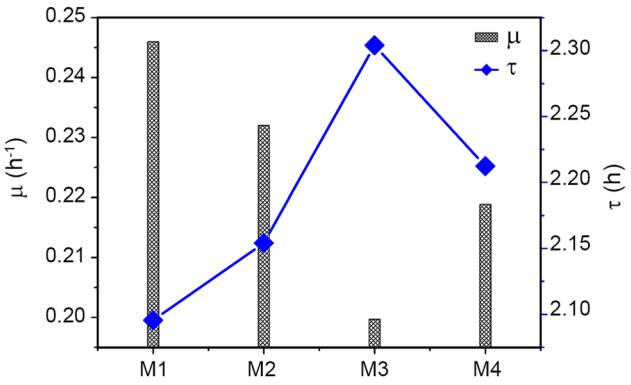

Fig. 8 Antibacterial activity of different composite membranes

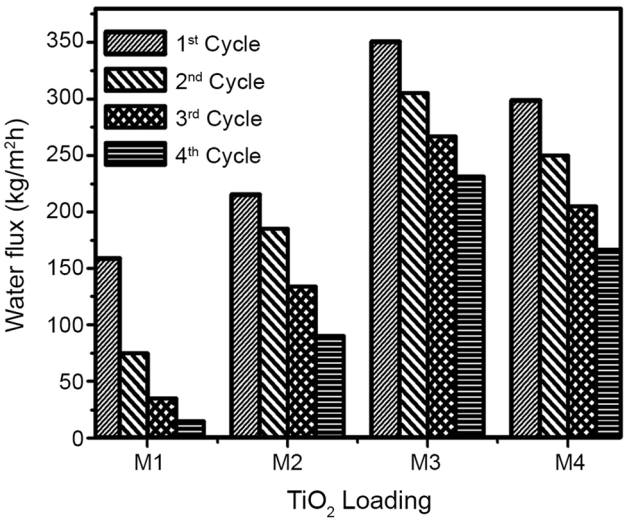

Fig. 9 Water flux value for different composite membranes before and after filtration of BSA bearing water

Permeate flux

Performance against BSA

A qualitative evaluation of the antifouling property of membranes was carried out by measuring the water flux with BSA as the model foulant. Incorporation of appropriate inorganic particles is an effective way to enhance the hydrophilicity and antifouling property. The water flux values before and after BSA filtration are shown in Fig. 9. An improvement in flux with an increase in TiO_2 loading from 0 to 0.01 g TiO_2/g PVDF is observed. This enhancement is due to the hydrophilic nature of TiO_2. For membrane M4, flux has declined due to agglomeration of TiO_2 particles [46, 47]. In the second set of runs after BSA filtration, it is observed that the decline in pure water flux is highest for pristine PVDF membrane compared to composite membranes. The same trend was followed for the third and fourth cycles with a small change in FRR suggesting the stability performance of the nanocomposite membrane. These results are in agreement with the results obtained from the XDLVO theory, where the energy barrier follows the order M3 > M4 > M2 > M1, so the deposition or blocking of membrane surface for M3 is minimal. The flux recovery ratio (FRR) of composite membranes is shown in Fig. 10a. The graph represents the increased value of FRR for modified membrane indicating better reuse, antifouling and cleaning property of the composite membrane.

The rejection percentage for various membranes is shown in Fig. 10b. This trend is expected because higher flux recovery ratio means less fouling of the membrane surface. Increase in nanoparticle loading reduces the roughness hence the foulant will not accumulate on the membrane surface rather it will be rejected easily resulting in a high flux.

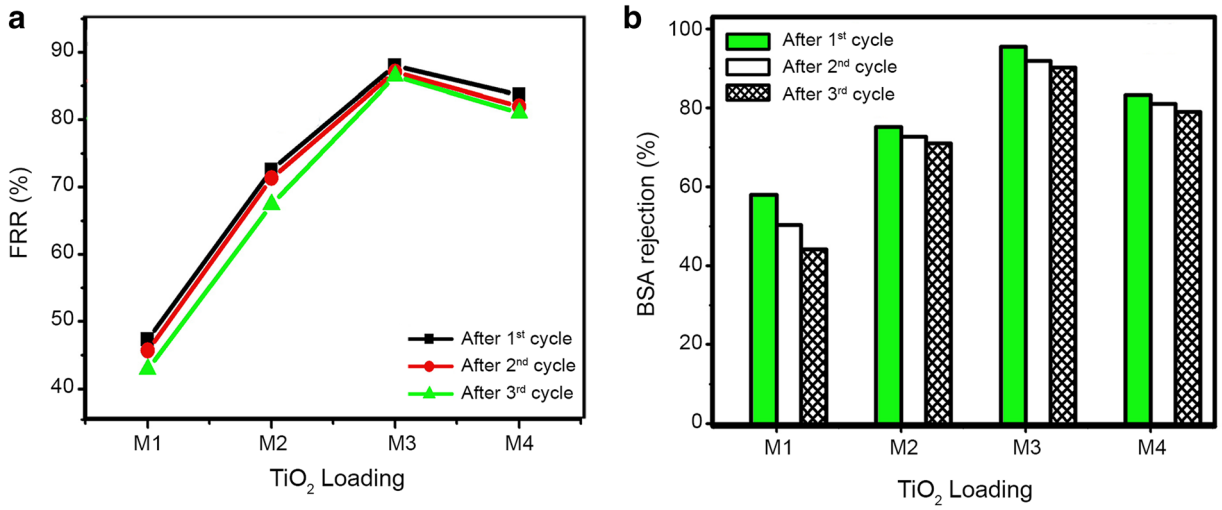

Fig. 10 FRR and % BSA rejection for different PVDF/TiO_2 composite membranes

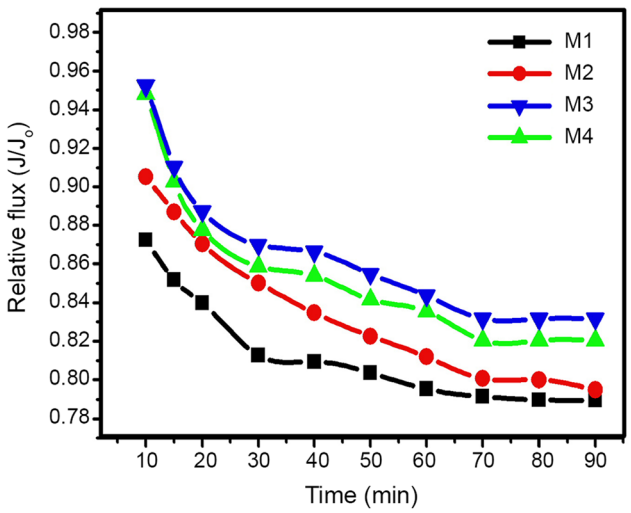

Fig. 11 Flux ratio during filtration of HA solution

Performance against HA

To further examine the antifouling property of nanocomposite membranes, ultrafiltration of HA was conducted. The variation of relative flux with time is shown in Fig. 11. The figure depicts a decrease in fouling tendency of PVDF/TiO_2 membrane compared to pure PVDF. A maximum resistance against fouling was observed for M3 membrane having the lowest contact angle (Table 2) and least roughness (Fig. 2). The probability of adsorption decreases on the membrane surface with the addition of TiO_2 nanoparticles which is a consequence of increasing membrane hydrophilicity. Adsorption of foulant is considered as the first step causing membrane fouling, and it is dependent on the physicochemical properties of both the membranes and foulants [48]. It is a well-known fact that hydrophobic surfaces have a higher tendency toward fouling, as a result, adsorption occurs relatively quickly for hydrophobic than hydrophilic surfaces [49]. The addition of TiO_2 nanoparticles decreased the roughness, so further mitigated the fouling. Thus it became significantly important to fabricate membrane with less roughness and improved hydrophilicity to enhance the performance as well as antifouling ability. Hence, based on the results of BSA and HA filtration it may be concluded that TiO_2-incorporated PVDF membranes possess better antifouling characteristic compared to pristine PVDF with the best result obtained for M3 membrane in both cases.

Hence, it can now be concluded that TiO_2 immobilized PVDF membranes exhibit good rejection and show the potential for water flux recovery. Also after deep investigation a comparison of the improved relative percentage of

Table 5 Comparison of the performance of inorganic-polymer nanocomposite membranes prepared in this work and those reported in the literature

Polymer	Solvent	Additive (wt%)	Nanoparticle (wt%)	Result	References
PVDF	NMP	Thermoexfoliated vermiculite blended poly(ether sulfone) (PES) (5–20 wt%)	–	CA approx 85°–52° Flux 330–476.4 (L/m^2 h) FRR 83.77% after 3 cycle	[50]
PVDF	DMAc (dimethylacetamide)	PVP (0.01) (polyvinylpyrrolidone)	Carbon nanotube (1 wt%) and graphite oxide (1 wt%)	CA approx 65° and 70° Flux 115 and 160 (L/m^2 h) FRR 72.8% and 85.1%	[51]
PVDF	DMAc	PVP (0.01)	Graphite oxide (0, 0.5, 1 and 2 wt%)	CA approx 71°–60° Flux 78–361.24 (L/m^2 h)	[52]
PVDF	DMAc	PVP (0.01)	Graphite oxide (0, 0.5, 1 and 2 g/L)	CA 81°–58° Flux 280–467.8 (L/m^2 h) FRR 42–85.7%	[53]
PES	DMF (*N,N*-dimethylformamide)	–	TiO_2 (0.45 wt%)	Cleaning efficiency 17–71% (approx) FRR 82%	[54]
PVDF	DMAc	PVP	Ag–TiO_2–APTES (0–0.5 g)	CA 81.8°–61.4° Rejection %(MB) 43.7–94.4	[55]
PVDF	DMAc	PVP	TiO_2 (0–5 wt%)	Flux 155–266 (L/m^2 h) Rejection %(BSA)-85–95	[56]
PVDF	NMP	–	TiO_2 (0–0.02 TiO_2/g PVDF)	CA 85.4°–70.2° Flux 158–350 (kg/m^2 h) FRR 57–95%	This work

CA contact angle, *MB* methylene blue

water flux, flux recovery ratio and contact angle for inorganic nanomaterial–PVDF hybrid membranes and PVDF/TiO_2 membranes in this work is listed in Table 5. It is seen that TiO_2–PVDF membrane presents a promising approach with the other PVDF composite membranes. Compared to other membranes reported in literature the cost of PVDF/TiO_2 membranes can be lower due to the absence of other additives such as PVP or PES and low cost of TiO_2 when compared to GO NPs and this may broaden the horizon for treatment of wastewater using membrane technology.

Conclusion

The incorporation of TiO_2 has enhanced hydrophilicity, reduced surface roughness and improved repulsive interaction energy barrier between the foulant and the membrane, thus resulting in a better antifouling ability of the membrane surface. The XRD spectra have confirmed successful incorporation of TiO_2 in the membrane matrix. At higher loading, aggregation of TiO_2 particles has resulted in increased surface roughness due to the formation of bumps leading to the reduction in their repulsive interaction and decrease in system's antifouling characteristics. The composite membrane with optimal TiO_2 loading (0.01 g TiO_2/g PVDF) has shown an excellent flux recovery ratio (approx. 95%) compared to other membranes when subjected to four cycles of use, thus indicating that membranes with an optimum TiO_2 loading can withstand fouling without affecting the flux. This membrane has exhibited the highest antifouling ability. Higher TiO_2 loading has resulted in reductions in active surface sites available for the killing of bacteria.

Acknowledgements The authors acknowledge Central Instrument Facility, IIT (BHU) for characterization facility.

Compliance with ethical standards

Conflict of interest The authors declare no conflict of interest.

References

1. Elimelech M, Phillip AW(2011)The future of seawater desalination: energy, technology, and the environment. Science 333:712–717
2. Salimi A, Yousefi AA (2013) Analysis method: FTIR studies of β-phase crystal formation in stretched PVDF films. Polym Test 22:699–704
3. Wang Q, Wang Z, Zhang J, Wang J, Wu Z (2014) Antifouling behaviours of PVDF/nano-TiO_2 composite membranes revealed by surface energetics and quartz crystal microbalance monitoring. RSC Adv 4:43590–43598
4. Lin T, Lu Z, Chen W (2015) Interaction mechanisms of humic acid combined with calcium ions on membrane fouling at different conditions in an ultrafiltration system. Desalination 357:26–35
5. Le-Clech P, Chen V, Fane TAG (2006) Fouling in membrane bioreactors used in wastewater treatment. J Membr Sci 284:17–53
6. Hong H, Peng W, Zhang M, Chen J, He Y, Wang F, Weng X, Yu H, Lin H (2013) Thermodynamic analysis of membrane fouling in a submerged membrane bioreactor and its implications. Bioresour Technol 146:7–14
7. Buonomenna MG, Macchi P, Davoli M, Drioli E (2007) Poly(vinylidene fluoride) membranes by phase inversion: the role the casting and coagulation conditions play in their morphology, crystalline structure and properties. Eur Polym J 43:1557–1572
8. Chang H, Qu F, Liu B, Yu H, Li K, Shao S, Li G, Liang H (2015) Hydraulic irreversibility of ultrafiltration membrane fouling by humic acid: effects of membrane properties and backwash water composition. J Membr Sci 493:723–733
9. Weis A, Bird MR, Nyström M, Wright C (2005) The influence of morphology, hydrophobicity and charge upon the long-term performance of ultrafiltration membranes fouled with spent sulphite liquor. Desalination 175:73–85
10. Kim DS, Kangand JS, Lee YM (2004) The influence of membrane surface properties on fouling in a membrane bioreactor for wastewater treatment. Sep Sci Technol 39:833–854
11. Mo J, Son SH, Jegal J, Kim J, Lee YH (2007) Preparation and characterization of polyamide nanofiltration composite membranes with TiO_2 layers chemically connected to the membrane surface. J Appl Polym Sci 105:1267–1274
12. Li JF, Xu ZL, Yang H, Yu LY, Liu M (2009) Effect of TiO_2 nanoparticles on the surface morphology and performance of microporous PES membrane. App Surf Sci 255:4725–4732
13. Li WY, Sun XL, Wen C, Lu H, Wang ZW (2013) Preparation and characterization of poly (vinylidene fluoride)/TiO_2 hybrid membranes. Front Env Sci Eng 7:492–502
14. Yang YN, Wang P (2006) Preparation and characterizations of new PS/TiO_2 hybrid membranes by sol–gel process. Polymer 47:2683–2688
15. Yan L, Hong S, Li ML, Li YS (2009) Application of the Al_2O_3–PVDF nanocomposite tubular ultrafiltration (UF) membrane for oily wastewater treatment and its antifouling research. Sep Purif Technol 66:347–352
16. Wang ZH, Yu HR, Xia JF, Zhang FF, Li F, Xia YZ, Li YH (2012) Novel GO-blended PVDF ultrafiltration membranes. Desalination 299:50–54
17. Brunet P, Lyon DY, Zodrow K, Rouch JC, Caussat B, Serp P, Remigy JC, Wiesner MR, Alvarez PJJ (2008) Properties of membranes containing semi-dispersed carbon nanotubes. Environ Eng Sci 25:565–575
18. Diebold U (2003) The surface science of titanium dioxide. Surf Sci Rep 48:53–229
19. Zhang X, Wang Z, Chen M, Liu M, Wu Z (2016) Polyvinylidene fluoride membrane blended with quaternary ammonium compound for enhancing anti-biofouling properties: effects of dosage. J Membr Sci 520:66–75
20. Raghupathi KR, Koodali RT, Manna AC (2011) Size-dependent bacterial growth inhibition and mechanism of antibacterial activity of zinc oxide nanoparticles. Langmuir 27:4020–4028
21. Subramaniam MN, Goh PS, Lau WJ, Tan YH, Ng BC, Ismail AF (2017) Hydrophilic hollow fiber PVDF ultrafiltration membrane incorporated with titanate nanotubes for decolourization of aerobically-treated palm oil mill effluent. Chem Eng J 316:101–110
22. Liu X, Chen Q, Lv L, Feng X, Meng X (2015) Preparation of transparent PVA/TiO_2 nanocomposite films with enhanced visible-light photocatalytic activity. Catal Commun 58:30–33
23. Almeida NA, Martins PM, Teixeira S, da Silva JAL, Sencadas V, Kühn K, Cuniberti G, Mendez SL, Marques PAAP (2016) TiO_2/graphene oxide immobilized in P(VDF-TrFE) electrospun

membranes with enhanced visible-light induced photocatalytic performance. J Mater Sci 51:6974–6986
24. Zhang M, Liao B, Zhou X, He Y, Hong H, Lin H, Chen J (2015) Effects of hydrophilicity/hydrophobicity of membrane on membrane fouling in a submerged membrane bioreactor. Bioresour Technol 175:59–67
25. Derjaguin B (1941) Theory of the stability of strongly charged lyophobic sols and the adhesion of strongly charged particles in solutions of electrolytes. Acta Physicochim URSS 14:633–662
26. Verwey EJ (1947) Theory of the stability of lyophobic colloids. J Phys Chem 51:631–636
27. Lin T, Lu ZJ, Chen W (2014) Interaction mechanisms and predictions on membrane fouling in an ultrafiltration system, using the XDLVO approach. J Membr Sci 461:49–58
28. Wang X, Zhou M, Meng X, Wang L, Huang D (2016) Effect of protein on PVDF ultrafiltration membrane fouling behavior under different pH conditions, interface adhesion force and XDLVO theory analysis. Front Env Sci Eng 10:12
29. Van Oss CJ (1995) Hydrophobicity of biosurfaces—origin, quantitative determination and interaction energies. Colloids Surf B 5:91–110
30. Safarpour M, Khataee A, Vatanpour V (2014) Preparation of a novel polyvinylidenefluoride (PVDF) ultrafiltration membrane modified with reduced grapheme oxide/titanium dioxide (TiO_2) nanocomposite with enhanced hydrophilicity and antifouling properties. Ind Eng Chem Res 53:13370–13382
31. Xu X, Yang Q, Wang Y, Yu H, Chen X, Jing X (2006) Biodegradable electrospun poly(L-lactide) fibers containing antibacterial silver nanoparticles. Eurp Polym J 42:2081–2087
32. Du JR, Peldszus S, Huck PM, Feng X (2015) Modification of membrane surfaces via microswelling for fouling control in drinking water treatment. J Membr Sci 475:488–495
33. Kim BS, Lee J (2016) Macroporous PVDF/TiO_2 membranes with three-dimensionally interconnected pore structures produced by directional melt crystallization. Chem Eng J 301:158–165
34. Oh SJ, Kim N, Lee YT (2009) Preparation and characterization of PVDF/TiO_2 organic–inorganic composite membranes for fouling resistance improvement. J Membr Sci 345:13–20
35. Meng N, Priestley RCE, Zhang Y, Wang H, Zhang X (2016) The effect of reduction degree of GO nanosheets on microstructure and performance of PVDF/GO hybrid membranes. J Membr Sci 501:169–178
36. Zhao C, Xu X, Chen J, Yang F (2013) Effect of graphene oxide concentration on the morphologies and antifouling properties of PVDF ultrafiltration membranes. J Environ Chem Eng 1:349–354
37. Zinadini S, Zinatizadeh AA, Rahimi M, Vatanpour V, Zangeneh H (2014) Preparation of a novel antifouling mixed matrix PES membrane by embedding graphene oxide nanoplates. J Membr Sci 453:292–301
38. Bae TH, Tak TM (2005) Effect of TiO_2 nanoparticles on fouling mitigation of ultrafiltration membranes for activated sludge filtration. J Membr Sci 249:1–8
39. Martins PM, Miranda R, Marques J, Tavares CJ, Botelho G, Lanceros-Mendez S (2016) Comparative efficiency of TiO_2 nanoparticles in suspension vs. immobilization into P(VDF–TrFE) porous membranes. RSC Adv 6:12708–12716
40. Damodar RA, Youa S, Chou H (2009) Study the self-cleaning, antibacterial and photocatalytic properties of TiO_2 entrapped PVDF membranes. J Hazard Mater 172:1321–1328
41. Shen F, Lu XF, Bian XK, Shi LQ (2005) Preparation and hydrophilicity study of poly (vinyl butyral)-based ultrafiltration membranes. J Membr Sci 265:74–84
42. He Y, Chen X, Dai F, Xu R, Yang N, Feng X, Zhao Y, Chen L (2018) Immobilization of poly(*N*-acryloylmorpholine) via hydrogen-bonded interactions for improved separation and antifouling properties of poly (vinylidene fluoride) membranes. React Funct Polym 123:80–90
43. Rincon AG, Pulgarin C (2003) Photocatalytical inactivation of *E. coli*, effect of (continuous intermittent) light intensity and of (suspended-fixed) TiO_2 concentration. Appl Catal B 44:263–284
44. Caballero L, Whitehead KA, Allen NS, Verran J (2009) Inactivation of *Escherichia coli* on immobilized TiO_2 using fluorescent light. J Photochem Photobiol A 202:92–98
45. Rahimpour A, Jahanshahi M, Rajaeian B, Rahimnejad M (2011) TiO_2 entrapped nano-composite PVDF/SPES membranes: preparation, characterization, antifouling and antibacterial properties. Desalination 278:343–353
46. Dutta AK, Egusa M, Kaminaka H, Izawa H, Morimoto M, Saimoto H, Ifuku S (2015) Facile preparation of surface *N*-halamine chitin nanofiber to endow antibacterial and antifungal activities. Carbohydr Polym 115:342–347
47. Liu J, Shen X, Zhao Y, Chen L (2013) Acryloylmorpholine-grafted PVDF membrane with improve protein fouling resistance. Ind Eng Chem Res 52:18392–18400
48. Li X, Fang X, Pang R, Li J, Sun X, Shen J, Han W, Wang L (2014) Self-assembly of TiO_2 nanoparticles around the pores of PES ultrafiltration membrane for mitigating organic fouling. J Membr Sci 467:226–235
49. Arsuaga JM, Lopez-Munoz MJ, Sotto A (2010) Correlation between retention and adsorption of phenolic compounds in nanofiltration membranes. Desalination 250:829–832
50. Orooji Y, Liang F, Razmjou A, Li S, Mofid R, Liu Q, Guan K, Liu Z, Jin W (2017) Excellent biofouling alleviation of thermoexfoliated vermiculite blended poly(ether sulfone) ultrafiltration membrane. ACS Appl Mater Interfaces 9:30024–30034
51. Zhang J, Xu Z, Mai W, Min C, Zhou B, Shan M, Li Y, Yang C, Wanga Z, Qiana X (2013) Improved hydrophilicity, permeability, antifouling and mechanical performance of PVDF composite ultrafiltration membranes tailored by oxidized low dimensional carbon nanomaterials. J Mater Chem A 1:3101
52. Xu Z, Zhang J, Shan M, Li Y, Li B, Niu J, Zhou B, Qian X (2014) Organosilane-functionalized graphene oxide for enhanced antifouling and mechanical properties of polyvinylidene fluoride ultrafiltration membranes. J Membr Sci 458:1–13
53. Wu T, Zhou B, Zhu T, Shi J, Xu Z, Hua C, Wang J (2015) Facile and low-cost approach towards a PVDF ultrafiltration membrane with enhanced hydrophilicity and antifouling performance via graphene oxide/water-bath coagulation. RSC Adv 5:7880–7889
54. Li X, Li J, Fang X, Bakzhan K, Wang L, Bruggen BV (2016) A synergetic analysis method for antifouling behavior investigation on PES ultrafiltration membrane with self-assembled TiO_2 nanoparticles. J Colloid Interface Sci 469:164–176
55. Peng Y, Yu Z, Pan Y, Zeng G (2017) Antibacterial photocatalytic self-cleaning poly(vinylidene fluoride) membrane for dye wastewater treatment. Polym Adv Technol 29:254–262
56. Cao X, Ma J, Shi X, Ren Z (2006) Effect of TiO_2 nanoparticle size on the performance of PVDF membrane. Appl Surf Sci 253:2003–2010